ARTICLE

Homochiral Hierarchical Molecular Assemblies through Dynamic Combination of Conformational States of a Single Chiral Building Block at the Liquid/Solid Interface

Received 00th January 20xx,
Accepted 00th January 20xx

DOI: 10.1039/x0xx00000x

Matsuhiro Maeda,[a] Kazuya Sato,[a] Steven De Feyter [b] and Kazukuni Tahara*[a]

We herein report the construction of homochiral, hierarchical self-assembled molecular networks (SAMNs) at the liquid/graphite interface using a single molecular building block, a chiral dehydrobenzo[12]annulene (cDBA) derivative with three chiral alkoxy and three hydroxy groups positioned in an alternating manner on the DBA core. The cDBA molecules form homochiral hierarchical SAMNs consisting of triangular clusters of several sizes, the size of which can be tuned by solvent polarity and solute concentration, reaching periodicities as large as 9.3 nm. We demonstrate the successful transmission of chirality information from the single molecular level to the hierarchical SAMN level, in a process that is mediated by dynamic self-sorting.

Introduction

The construction of homochiral hierarchical molecular assemblies has attracted great interest[1] because these chiral assemblies offer potential applications in chiral molecular recognition[2,3] and enantioselective reactions.[4] One of the key strategies for the construction of such intricate molecular assemblies is to utilize the successful transmission of chirality information from the single molecular level to the supramolecular level. Many investigations have established such a design strategy for various molecular systems in three-dimensional space,[5] *i.e*. metal complexes,[6–8] supramolecular polymers,[9,10] and gels.[11,12]

Control of the supramolecular chirality of self-assembled molecular networks (SAMNs)[13] on surfaces is of keen interest too.[14–21] Homochiral SAMNs can be constructed by using chiral molecular building blocks.[22,23] Moreover, external factors, such as chiral solvents[24–26] and electric fields[27] are known to bias the supramolecular chirality of SAMNs formed by achiral (prochiral) molecules. Chirality induction[22,28,29] and amplification[30] in SAMNs are also reported. A recent study demonstrated that homochiral SAMNs can be used as preorganized monomers for the synthesis of homochiral 2D covalent organic structures through chirality information transmission.[31–34] Though there are a few reports on chirality control of hierarchical molecular assemblies on metal substrates in ultrahigh vacuum (UHV) conditions,[35,36] such is not reported at the liquid/solid interface, probably because of its environmental complexity, requiring well-designed systems. Typically, the periodicity of homochiral SAMNs at the liquid/solid interface is a few nm only. Scanning tunneling microscopy (STM) is able to characterize the structure and chirality of SAMNs at the nanoscale with submolecular resolution.[37,38]

The construction of hierarchical SAMNs has been achieved by a self-sorting process involving several molecular building blocks.[39–41] This process involves hierarchical intermolecular recognition through a combination of different types of non-covalent interactions with multiple interaction sites and the size and shape of the molecular building blocks.[42–44] The process involving several molecular components is called social self-sorting.[45] The self-sorting also occurs for a single molecular component. In this case, the hierarchical SAMNs consist of the same molecular building block with different intermolecular interacting groups and/or molecular conformations. Most investigations are conducted on metal surfaces in UHV conditions by regulating the molecular surface coverage, in which hierarchical SAMNs are formed by the same molecular building block yet having different intermolecular interacting groups.[46–51] At the liquid/solid interface, there are two reports on the construction of hierarchical SAMNs formed by the dynamic combination of the conformational states of a single molecular component.[52,53] A challenge is the chirality control of these hierarchical SAMNs. This requires the development of a sophisticated design strategy that enables control over not only the structure but also the chirality of the hierarchical SAMNs.

We recently reported on the construction of a hierarchical SAMN at the liquid/graphite interface through self-sorting using dehydrobenzo[12]annulene (DBA) derivative **DBA-OC14-OH** having hydroxy groups and alkoxy chains arranged in an alternating manner (Fig. 1a).[53] Through the interplay of van der Waals and hydrogen bonding interactions, the **DBA-OC14-OH**

[a] *Department of Applied Chemistry, School of Science and Technology, Meiji University, 1-1-1 Higashimita, Tama-ku, Kawasaki, Kanagawa, 214-8571, Japan E-mail: tahara@meiji.ac.jp*
[b] *Division of Molecular Imaging and Photonics, Department of Chemistry, KU Leuven, Celestijnenlaan 200 F, 3001 Leuven, Belgium.*

Electronic Supplementary Information (ESI) available: Details of synthesis of the cDBAs, additional STM images, STM image analysis, details of MM and MD calculations ^{1}H and ^{13}C NMR spectra of new compounds. See DOI: 10.1039/x0xx00000x

molecules form hierarchical triangular clusters by the combination of the four conformational states, the latter being defined by the number of physisorbed alkoxy chains (m = 0, 1, 2, 3, Fig. 2a). The size of the triangular clusters defined by the number of the DBA molecules at each side of the cluster (n) can be controlled from 2 to 15 by the solvent polarity. Moreover, the hierarchical SAMNs are chiral while both mirror-image structures appear with equal probability (Figs. 2a, S1 and S2).

Based on our previous findings, we here envision that it should be possible for hierarchical SAMNs to show single-handedness by bestowing chiral information to a molecular building block. We report the formation of homochiral chiral triangular clusters of various sizes through the dynamic combination of the different conformational states of newly designed molecules, enantiopure **cDBA-OC14(*S*)-OH** and **cDBA-OC14(*R*)-OH** at the liquid/graphite interface (Fig. 1a). Careful design, in combination with optimized experimental conditions, leads to the successful transfer of chiral information at the single molecule level to mono-component homochiral complex hierarchical structures, with periodicities that exceed 9 nm, the size of which is tuned by solvent polarity and solute concentration.

Results and discussion

With the ambition in mind of creating homochiral mono-component hierarchical self-assembled molecular networks, new molecules, i.e. **cDBA-OC14(*S*)-OH** and **cDBA-OC14(*R*)-OH**, were designed with on the one hand alkoxy groups with a methyl group substituted at the 2-position rendering these chiral, and on the other hand hydroxy groups. The alkoxy and hydroxy groups are positioned on the DBA core in an alternating manner (Fig. 1a). So, except for the chiral center, the structures of the chiral DBAs are identical to **DBA-OC14-OH**. It was expected that upon adsorption on graphite, the chiral DBA (C_{3h} symmetry (m = 3)) will adopt a single chiral configuration driven by the steric repulsion between the methyl groups at the stereogenic centers and the graphite surface (Figs. 1b,c). In other words, we assumed that the chiral DBA would adsorb preferentially, if not exclusively, always with the same face on the surface, also for other conformational states with fewer numbers of adsorbed alkoxy chains (m = 1 and 2) (Fig. 2b). In contrast, no transmission of chiral information was expected to occur for the conformational state where no alkoxy chains (m = 0) are adsorbed on the surface. Note that in analogy with **DBA-OC14-OH**, when the chiral DBA would form the triangular clusters (Fig. 2c), the number of adsorbed chiral chains (m) is different depending on the position of the molecule in the triangular clusters (top: m = 2, side: m = 1, and inside: m = 0). Therefore, the number of adsorbed chiral chains per triangular cluster should decrease upon increasing cluster size (Fig. S8), and potentially also the control of supramolecular chirality.

cDBA-OC14(*S*)-OH and **cDBA-OC14(*R*)-OH** were synthesized from **DBA-OTBS-OMOM** in two-step synthetic transformations (see ESI).[29] For SAMN preparation at the liquid/solid interface, we prepared a solution of the chiral DBA in 1,2,4-trichlorobenzene (TCB), 1-hexanoic acid (HA), or their mixture. We chose these solvents because of the following reasons. For achiral **DBA-OC14-OH**, co-adsorption of HA molecules is an essential element in forming the hierarchical SAMNs through hydrogen bonding interactions between the carboxy group of the HA molecule and the hydroxy group of the DBA molecule.[53] Moreover, our previous study reported that the size of the triangular clusters was modulated by solvent polarity using mixtures of TCB and HA in different ratios. We set different solute concentrations ranging from 3.0×10^{-6} to 1.0×10^{-2} M to check concentration-dependent structural changes. The sample solution (40 µL) was poured into a liquid cell which was attached to a freshly cleaved surface of highly oriented pyrolytic graphite (HOPG). An annealing treatment was applied at the liquid/graphite interface at 80 °C for 3 h to stimulate SAMN formation. After the annealing treatment, the liquid cell was allowed to cool down to room temperature, and then STM imaging was performed at room temperature. ~~As we expected no differences in the self-assembly behavior for the *R* and *S* isomers, except for the supramolecular chirality of the SAMNs,[22,23] the most detailed investigation was only performed for one of the enantiomers, i.e. **cDBA-OC14(*S*)-OH**. Nevertheless, the results for **cDBA-OC14(*R*)-OH** are equivalent and, as expected mirror symmetric. The data on **cDBA-OC14(*R*)-OH** are therefore presented in the Supporting Information.~~

As we expected, there were no differences in the self-assembly behavior for the R and S isomers, except for the supramolecular chirality of the SAMNs.[22,23] The most detailed investigation was only performed for one of the enantiomers, i.e., **cDBA-OC14(S)-OH**. Nevertheless, the results for cDBA-OC14(R)-OH are equivalent and, as expected, mirror-symmetric. The data on **cDBA-OC14(*R*)-OH** are presented in the Supporting Information.

We constructed the network models by geometry optimization of the DBA molecules on bilayer graphene sheets using molecular mechanics (MM) simulations with the COMPASS force field under periodic boundary conditions. Further details on the STM observation and MM simulations are described in ESI.

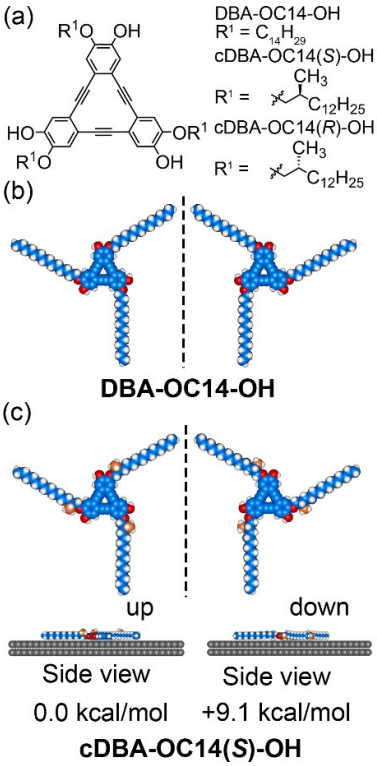

Figure 1. (a) Chemical structures of **DBA-OC14-OH**, **cDBA-OC14(*S*)-OH**, and **cDBA-OC14(*R*)-OH**. (b) Two isoenergetic enantiomorphic adsorption motifs of **DBA-OC14-OH** on bilayer graphene sheets optimized by molecular mechanics (MM) simulations. The bilayer graphene sheet is omitted for clarity. (c) Two adsorption configurations of **cDBA-OC14(*S*)-OH** on bilayer graphene sheets optimized by MM simulations. "Up" and "down" refers to the orientation of the methyl groups on the 2-position of the alkoxy groups with respect to the substrate underneath.

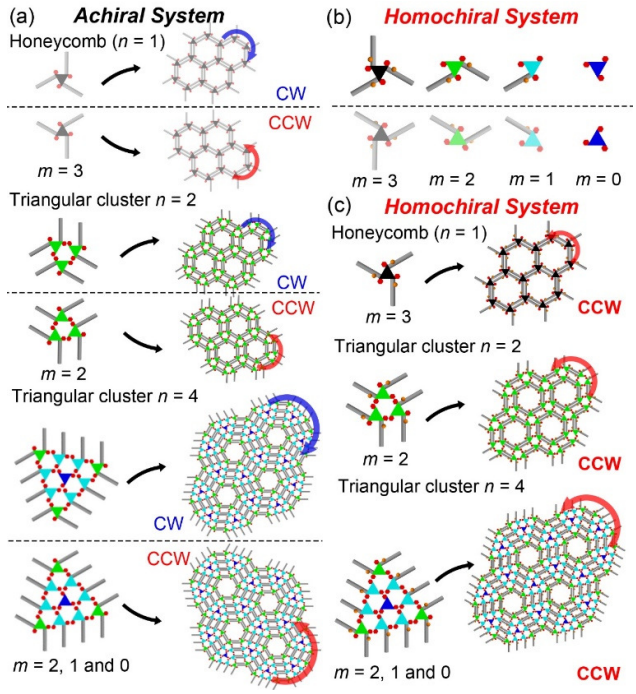

Figure 2. (a) Schematic illustration of a honeycomb structure (hypothetical) and triangular clusters (n = 2 and 4) formed by achiral **DBA-OC14-OH**. The n refers to the number of the DBA molecules at each side of the triangular cluster. Always CW and CCW structures appear in separate domains. The triangular cores of the DBA molecules with different conformational states are colored dark gray (m = 3), light green (m = 2), turquoise (m = 1), and blue (m = 0). (b) Schematic illustration of the four conformational states of **cDBA-OC14(*S*)-OH** with the different numbers (m) of adsorbed alkyl chains. The alkyl chains orienting to a solution phase are omitted for clarity. We defined CW (upper row) and CCW (lower row) rotations at the single molecular level based on the alkyl chain orientations. (c) Schematic drawings of the formation of the homochiral hierarchical molecular self-assemblies of **cDBA-OC14(*S*)-OH**.

Self-assembly from 1,2,4-trichlorobenzene

In TCB, **cDBA-OC14(*S*)-OH** exclusively forms a honeycomb structure with one DBA molecule at each corner at all solute concentrations (Figs. 3a and S3), in contrast to achiral **DBA-OC14-OH** which forms a honeycomb structure with a cluster consisting of four DBA molecules at each corner (Fig. S1).[53] In STM images, a π-conjugated core often appears brighter because of its higher tunneling efficiency. Thus, the bright triangular features are the π-conjugated cores of the cDBA. The lines bridging the cDBA cores are adsorbed alkyl chains that run parallel to the main symmetry axes of the graphite substrate underneath. The alkyl chains show a [1+1] type interaction. Unit cell parameters are $a = b = 5.0 \pm 0.1$ nm and $\gamma = 60 \pm 1°$. The supramolecular chirality of the honeycomb structure is discerned by the alkyl chain orientation (clockwise (CW) or counterclockwise (CCW) orientation) at the rim of the hexagonal pore (Fig. S4). Moreover, this chirality is differentiated by the angle α between the unit cell vector a and one of the normals of the main symmetry axes of graphite (Fig. S2). For the analysis of the chirality of the honeycomb structure, we used more than 26 STM images (80 nm × 80 nm) at each solute concentration (Table S1). Only the CCW honeycomb structure covers the surface. Moreover, the angle α values (Fig. 3a) determined from more than 4 images are all negative at all concentrations. These analyses confirm that the honeycomb structures formed by **cDBA-OC14(*S*)-OH** are globally homochiral, with CCW orientation. This is in agreement with the favorable orientation of the methyl groups, determined at the single molecular level, of **cDBA-OC14(*S*)-OH** adsorbed on graphite (Fig. 1c). Moreover, the network model optimized by MM simulation is shown in Fig. 3b, in which we assume that the methyl groups attached at the stereogenic centers orient to the solution phase. The details on the network modeling are described in ESI (Fig. S4).

In contrast to the case of achiral **DBA-OC14-OH**, the honeycomb structure for chiral **cDBA-OC14(*S*)-OH** consists of single DBA molecules at each corner. We consider that the formation of a tetrameric cluster is unfavorable for **cDBA-OC14(*S*)-OH** because of the steric hindrance arising from non-uniform orientations of the stereogenic methyl groups with respect to the graphite surface in the tetrameric cluster as discussed in ESI (Fig. S5).

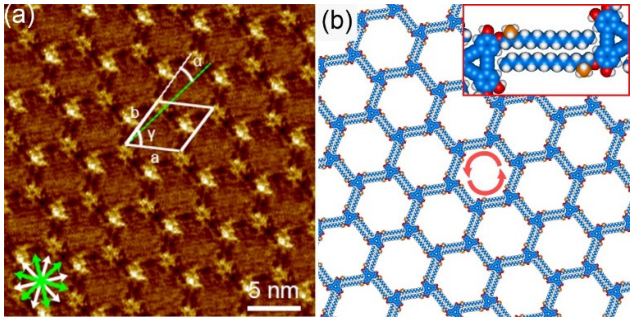

Figure 3. SAMNs formed by **cDBA-OC14(*S*)-OH** at the TCB/graphite interface. (a) STM image of a honeycomb structure (1.0×10^{-4} M, I_{set} = 200 pA, and V_{bias} = −0.43 V) and (b) corresponding molecular models optimized by MM calculation on bilayer graphene sheets. In the MM models in (b), the bilayer graphene sheets were omitted for clarity. Color codes in (b): blue; carbon atoms of **cDBA-OC14(*S*)-OH**, orange; carbon atoms of the methyl groups attached to the stereogenic centers, red; oxygen atoms, and white; hydrogen atoms. An inset in (b) highlights a [1+1] alkyl chain interaction mode.

Self-assembly from 1-hexanoic acid

Contrary to the SAMN formation in TCB, concentration-dependent polymorphism is observed at the HA/graphite interface. At a low solute concentration of 6.0×10^{-6} M, a triangular cluster structure (n = 2) formed by three **cDBA-OC14(*S*)-OH** molecules having the same conformational state (m = 2) with two physisorbed alkyl chains is observed (Figs. 4a,b). The cDBA molecules in the trimeric cluster are linked by four alkyl chains and two co-adsorbed HA molecules, located in the middle of the alkyl chain linkages. These align parallel to the main symmetry axis of graphite underneath (Fig. S6). The triangular cluster is sustained by hydrogen bonding interactions between the hydroxy group of the cDBA molecule and a HA molecule. Unit cell parameters are $a = b = 6.4 \pm 0.1$ nm and $\gamma = 60.0 \pm 0.5°$. In the case of achiral **DBA-OC14-OH**, the same triangular cluster structure (n = 2) is formed, while both CW and CCW domains appear with equal probability. On the other hand, the chirality of all triangular clusters formed by **cDBA-OC14(*S*)-OH** in 22 large area STM images (80 nm × 80 nm) is exclusively CCW. This is also supported by a mean angle α value of $-5.0 \pm 0.2°$ (Fig. S7). All cDBA molecules with the configurational state m = 2 in the CCW structure adopt the same molecular orientation in which all methyl groups orient to the solution phase (Fig. 1c, left). The favorable molecular orientation on the graphite surface renders the SAMN homochiral. When the concentration is increased to the range of 1.0×10^{-5} to 5.0×10^{-3} M, small domains of the triangular clusters of various sizes (n = 2 to 5) and a linear pattern emerge (Fig. S9). The triangular clusters larger than n = 3 consist of a combination of the molecules with three different molecular conformational sates (m = 0, 1, and 2). The linear patterns consist of **cDBA-OC14(*S*)-OH** of the conformational state m = 2 (Figs. 4b,c). Unit cell parameters of the linear structure are $a = 1.4 \pm 0.1$ nm, $b = 5.4 \pm 0.1$ nm, and $\gamma = 76 \pm 1°$. At the highest concentration of 1.0×10^{-2} M, a densely packed structure consisting of the conformational state without physisorbed alkoxy chain (m = 0) appears (Figs. 4e,f). Unit cell parameters are $a = b = 1.36 \pm 0.05$ nm and $\gamma = 60.2 \pm 0.8°$. The angle α value is always negative giving a mean value of $-18 \pm 2°$. In the dense structure, all DBA molecules assemble through hydrogen bonding interactions. The alkyl chains of the DBA molecules orient to the solution phase and are solvated. Notably, the dense structure transforms to the linear pattern during STM tip scanning (Fig. S10). This implies that the dense structure is destabilized by STM tip scanning. It should be noted that the dense structure of **cDBA-OC14(*S*)-OH** is homochiral too, despite the fact that the chiral chains are not adsorbed on the surface (Fig. S11). This contrasts a previous report on the SAMN of an isophthalic acid derivative containing a chiral diacetylene unit in which supramolecular chirality disappears by the desorption of the chiral side chain from the substrate.[54] The chiral information of the chains will not be transferred to the dense structure because of their conformational freedom in the solution phase (Fig. S12). Another factor plays a role in chirality induction in the dense structure. We consider that the dense structure is formed from precursor states that have alkyl chains in contact with the substrate. Indeed, a linear structure observed at room temperature even at the highest concentration without annealing treatment is homochiral as well (Fig. S13). It is not surprising that on-surface molecular orientations are preserved through the hydrogen bonding interactions even after the chiral alkyl chains are desorbed from the surface. The present observation features a chirality memory effect, which has been scarcely observed in SAMNs.[55,56]

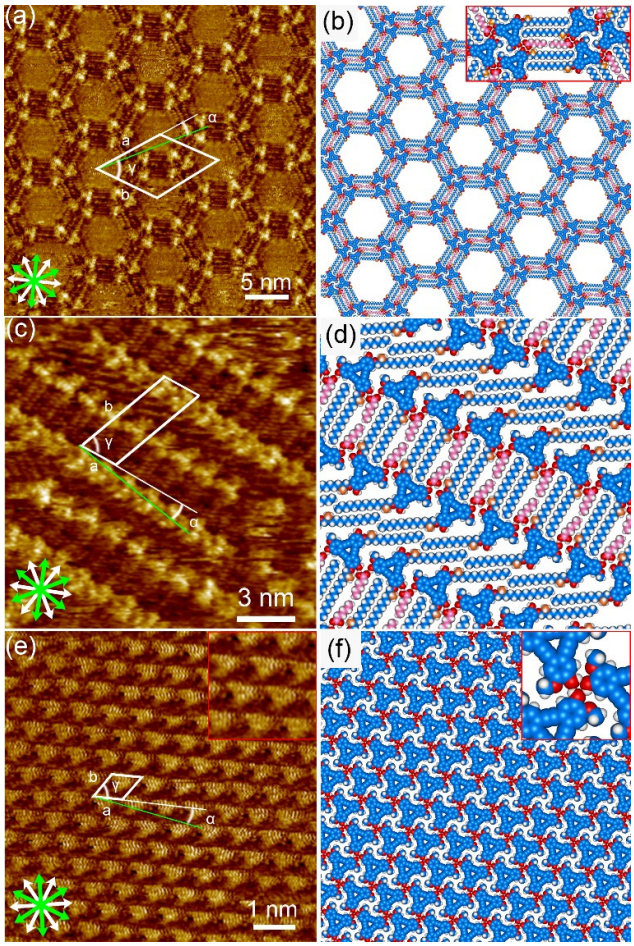

Figure 4. SAMNs formed by **cDBA-OC14(*S*)-OH** at the HA/graphite interface. (a) STM image of a triangular cluster (n = 2, 6.0×10^{-6} M, I_{set} = 250 pA, and V_{bias} = −0.44 V) and (b) corresponding molecular models optimized by MM calculation on bilayer graphene sheets. An inset in (b) highlights alkyl chain interaction modes involving co-adsorbed HA molecules. (c) STM image of a linear structure (1.0×10^{-4} M, I_{set} = 300 pA, and V_{bias} = −0.41 V) and (d) corresponding molecular models optimized by MM calculation on bilayer graphene sheets. (e) STM image of a dense structure (1.0×10^{-2} M, I_{set} = 250 pA, and V_{bias} = −0.48 V) and (f) corresponding molecular models optimized by MM calculation on bilayer graphene sheets. An inset in (e) shows a digitally zoomed image of a dense structure. An inset in (f) highlights cyclic hydrogen bonding interactions of the hydroxy groups which determine the molecular orientations. In the MM models, the bilayer graphene sheets and the alkoxy chains of the cDBA molecules orienting to the solution phase were omitted for clarity. Color codes in (b), (d), and (f): blue; carbon atoms of **cDBA-OC14(*S*)-OH**, orange; carbon atoms of the methyl groups attached to the stereogenic centers, magenta; carbon atoms of the co-adsorbed HA molecule, red; oxygen atoms, and white; hydrogen atoms.

Self-assembly from mixtures of 1,2,4-trichlorobenzene and 1-hexanoic acid

STM observations in pure TCB and HA solvents reveal that **cDBA-OC14(*S*)-OH** forms various, yet homochiral SAMNs consisting of combinations of the conformational states (m = 0 to 3). Previously, we reported that the achiral **DBA-OC14-OH** molecules produced the hierarchical structure consisting of the triangular cluster of n = 12 as a major component and those of similar sizes (n = 10 to 14) at an optimized molar fraction of TCB and HA and concentration.[53] Therefore, we hypothesized that the size of the homochiral hierarchical triangular clusters could also be controlled by tuning the solvent polarity using a mixture of TCB and HA at different mixing ratios and solute concentration. To examine this possibility, we used solutions of **cDBA-OC14(*S*)-OH** in TCB and HA mixed in various molar fractions (X_{HA}; 0.020–0.50 and X_{TCB}; 0.98–0.50) and of different concentrations ranging from 1.0×10^{-4} to 1.0×10^{-2} M.

Statistical analysis of the size distributions of the triangular clusters formed in a mixture of TCB and HA is summarized in Table 1. We also analyzed the chirality of the triangular clusters at each condition.

At an X_{HA} of 0.50, **cDBA-OC14(*S*)-OH** exclusively forms the smallest triangular cluster (n = 2) structure at all concentrations similar to that in pure HA of low concentration. At an X_{HA} of 0.80 at a concentration of 5.4×10^{-4} M, the domains of two triangular cluster structures of n = 2 and 4 coexist (Figs. 5a,b), where the typical domain sizes are over 80 nm × 80 nm for the n = 2 domain and ca. 50 nm × 50 nm for the n = 4 domains. The unit cell parameters of the triangular cluster structure of n = 4 are a = b = 9.25 ± 0.07 nm and γ = 60.1 ± 0.6°. Based on the orientations of the alkyl chains at the rim of the hexagonal pore in the larger triangular cluster (n = 4), only CCW structures are observed. A mean α value of –4.6 ± 0.7° also supports that the triangular cluster (n = 4) structure is homochiral (Figs. 5 and S14). In most of the n = 4 clusters, the central molecules of the conformational state m = 0 are missing. All molecules in this structure adopt the same orientation at the single molecular level with respect to the surface regardless of the conformational state (Fig. 1c, left). To enlarge the size of triangular clusters, we tested solutions at higher HA fraction and DBA concentrations (Figs. S15 and S16). At an X_{HA} of 0.90 and a concentration of 1.0×10^{-2} M, the triangular clusters (n = 2 to 10) are observed, though these clusters are randomly arranged (Fig. 6). Due to a lack of periodicity, the chirality of these clusters is not determined using the direction of the alkyl chains or the angle α. Instead, we analyzed the orientation of each triangular cluster with respect to one of the main symmetry axes of graphite. Statistical analysis based on 10 large area STM images (80 nm × 80 nm) indicates that these triangular clusters have the same chiral orientation with respect to the substrate lattice (Fig. S17). Therefore, we conclude that all SAMNs of **cDBA-OC14(*S*)-OH** are homochiral.

We also investigated the formation and supramolecular chirality of SAMNs formed by **cDBA-OC14(*R*)-OH** at the liquid/graphite interfaces. As expected, the self-assembly behavior of the *R*-isomer is the same as that of the *S*-isomer, except for the fact that the supramolecular chirality of all SAMNs is opposite (CW orientation). The details are described in ESI.

Table 1. Size distributions of the triangular clusters formed by **cDBA-OC14(*S*)-OH** at the interface between a mixture of TCB and HA at different molar fractions and graphite.

concentration (M)	X_{HA}	on-surface size distribution of triangular clusters (%)[a]								
		n = 2	*n* = 3	*n* = 4	*n* = 5	*n* = 6	*n* = 7	*n* = 8	*n* = 9	*n* = 10
1.0×10^{-4}	0.50	100	-	-	-	-	-	-	-	-
	0.80	100	-	-	-	-	-	-	-	-
	0.90	74.0 ± 12.0	6.2 ± 2.8	17.4 ± 8.3	2.4 ± 2.1	0.0	0.0	0.0	0.0	0.0
5.4×10^{-4}	0.50	100	-	-	-	-	-	-	-	-
	0.80	19.4 ± 4.5	0.0	80.6 ± 4.5	0.0	0.0	0.0	0.0	0.0	0.0
	0.90	13.8 ± 3.0	10.2 ± 0.9	51.7 ± 1.2	20.5 ± 2.8	2.7 ± 1.5	1.1 ± 0.2	0.0	0.0	0.0
4.5×10^{-3}	0.50	100	-	-	-	-	-	-	-	-
	0.80	3.0 ± 2.8	1.0 ± 0.4	49.8 ± 12.1	23.0 ± 1.7	11.5 ± 4.4	10.1 ± 5.3	0.8 ± 1.0	0.8 ± 1.2	0.1 ± 0.1
	0.90	0.0	4.6 ± 1.7	38 ± 5.3	27.3 ± 4.1	11.6 ± 2.2	1.5 ± 2.2	3.9 ± 1.6	0.8 ± 0.5	0.4 ± 0.3
1.0×10^{-2}	0.50	100	-	-	-	-	-	-	-	-
	0.90	0.7 ± 0.8	1.8 ± 1.3	32 ± 1.6	30.4 ± 6.4	15.0 ± 2.3	14.2 ± 3.4	3.9 ± 1.7	1.2 ± 0.4	0.7 ± 0.7
	0.99	0	0.3 ± 0.9	21.1 ± 1.8	29.0 ± 6.5	21.7 ± 1.8	17.4 ± 5.9	5.9 ± 1.4	2.5 ± 1.4	2.2 ± 1.5

[a]For the statistical analysis, more than 19 large area STM images (80 nm × 80 nm) were used for each condition.

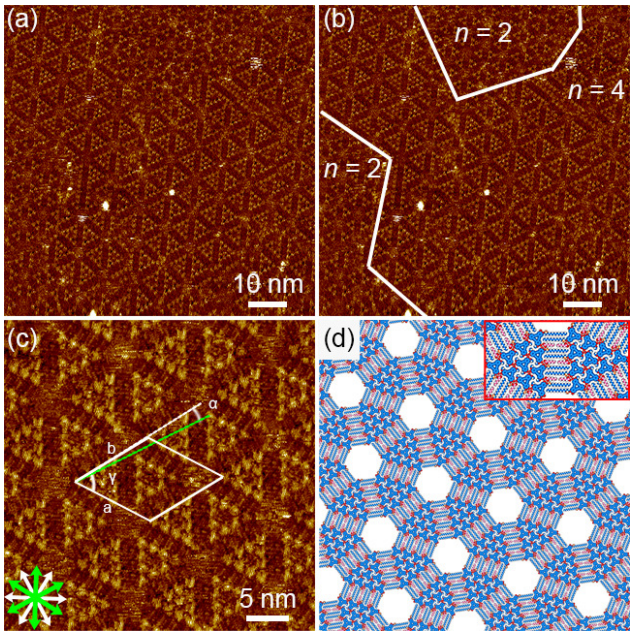

Figure 5. (a, b) STM images of hierarchical triangular cluster (n = 2 and 4) structures at an X_{HA} of 0.80 at a concentration of 5.4 × 10^{-4} M (I_{set} = 200 pA, V_{bias} = –0.41 V). In (b), numbers corresponding to n are overlayed. (c) STM image of a triangular cluster (n = 4) formed by **cDBA-OC14(*S*)-OH** at an X_{HA} of 0.80 at a concentration of 5.4 × 10^{-4} M (I_{set} = 200 pA, and V_{bias} = −1.20 V) and (d) corresponding molecular models optimized by MM calculation on bilayer graphene sheets. In the MM models in (d), the bilayer graphene sheets and the alkoxy chains orienting to the solution phase are omitted for clarity. An inset in (d) highlights an alkyl chain interaction part. Color codes in (d): blue; carbon atoms of **cDBA-OC14(*S*)-OH**, orange; carbon atoms of the methyl groups attached to the stereogenic centers, magenta; carbon atoms of the co-adsorbed HA molecule, red; oxygen atoms, and white; hydrogen atoms.

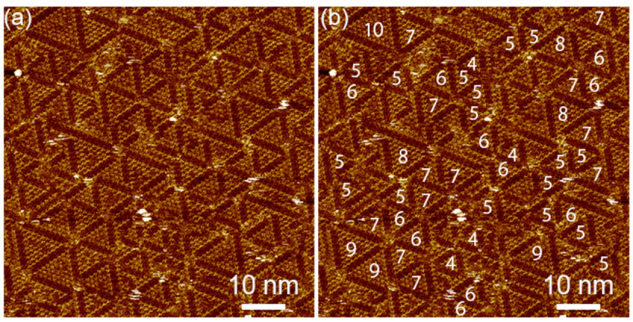

Figure 6. (a, b) STM images of hierarchical triangular cluster (n = 3 to 10) structures (X_{HA} = 0.90 at a concentration of 1.0 × 10^{-2} M after annealing treatment, I_{set} = 200 pA, V_{bias} = –0.40 V). In (b), numbers corresponding to n are overlayed.

Contrary to the case of achiral **DBA-OC14-OH**,[53] the triangular clusters formed by chiral **cDBA-OC14(*S*)-OH** are smaller than n < 11 even at the higher X_{HA} (0.99) and concentration values (1.0 × 10^{-2} M), showing clearly that the formation of the larger triangular clusters is unfavorable for the cDBA molecules. We ascribe it to an additional energy penalty for the cDBA molecule to adopt conformational states m = 0 and m = 1 as well, in which cDBA molecules are closely packed and linked by hydrogen-bonding interactions. With increasing cluster size, more cDBA with conformational states m = 0 and m = 1 are involved to form the cluster. For example, for n = 6 cluster, six cDBA molecules are surrounded by the rim consisting of twelve cDBA of m = 1 and only three cDBA of m = 2 (Fig. S18). We consider that the methyl groups attached at the stereogenic centers suffer from steric repulsion with those of the neighboring molecules because of the small intermolecular space. Under an adsorption-desorption equilibrium at the interface, the solvation energy will also influence the SAMNs formation.[57] Thus, the solvation energies of the DBA derivatives in HA are estimated by molecular dynamics (MD) simulations. The solvation energy of **cDBA-OC14(*S*)-OH** in HA is larger than that for **DBA-OC14-OH** by 2.2 kcal/mol (see ESI), which supports the observation that conformational states m = 0 and m = 1 are less common for **cDBA-OC14(*S*)-OH** structures compared to **DBA-OC14-OH**. We consider that one or more of these influence(s) the unfavorable formation of the structures composed of the conformational state of m = 0 for the chiral DBA molecule.

Conclusions

In conclusion, we designed and synthesized **cDBA-OC14(*S*)-OH** and **cDBA-OC14(*S*)-OH** with three chiral alkoxy chains and hydroxy groups for the construction of homochiral hierarchical molecular self-assemblies at the liquid/graphite interfaces. By introducing the chiral center, we succeeded in exclusively forming self-assembled molecular networks of one handedness, ranging from simple honeycomb lattices with two molecules per unit cell, to complex hierarchical self-assembled networks with tens of molecules in the repetitive motif, depending on concentration and solvent composition. Chiral information at the single molecule level is effectively transferred, even in those cases where the alkoxy chains containing the chiral center are oriented away from the substrate.

In TCB, the chiral DBA exclusively forms the homochiral honeycomb structure. Each corner of the honeycomb structure contains only one cDBA molecule in contrast to achiral DBA which also forms a hexagonal pattern but with a tetrameric cluster consisting of both enantiomers, at the corner. A

tetramer cannot be constructed by molecules of the same handedness, showing the different outcome between homochiral and mixed cases.

In HA, the chiral DBA produces a homochiral triangular cluster (n = 2) and dense structures depending on the solute concentration. The homochirality of the dense structure is attributed to a chiral memory effect. A homochiral triangular cluster (n = 4) and hierarchical structures consisting of triangular clusters with several sizes are formed by changing the polarity of the solvent (mixture of HA and TCB) and solute concentration. However, in the case of the chiral DBA, the larger clusters with n > 10 are not formed, which is in contrast to **DBA-OC14-OH**. The absence of large triangular clusters for the chiral DBA is attributed to unfavorable conformational states (m = 0 and 1) on the graphite surface and/or solvation issues.

The present study demonstrates the potential to induce and control chirality in hierarchical molecular self-assemblies using self-sorting, and is a valuable addition to the toolbox of 2D crystal engineering for the construction of homochiral intricate molecular self-assemblies. We believe that larger homochiral hierarchical self-assemblies may be possible by further optimization of the molecular structure (the position of stereogenic centers) or the use of enantiopure solvent.

Conflicts of interest

There are no conflicts to declare.

Acknowledgements

This work was supported by JSPS KAKENHI Grant Number JP20H02553, KU Leuven (C14/19/079), and Research Foundation – Flanders (G0H2122N, G0E3422N). This work was in part supported by FWO and F. R. S.-FNRS under the Excellence of Science EOS program (project 40007495). We would like to thank Prof. Yoshito Tobe (National Yang Ming Chiao Tung University) for his useful advice.

Notes and references

1 P. Peluso and B. Chankvetadze, *Chem. Rev*. 2022, **122**, 13235–13400.
2 J. A. A. W. Elemans, S. Lei and S. De Feyter, *Angew. Chem., Int. Ed.*, 2009, **48**, 7298–7333.
3 Y. Tobe, K. Tahara and S. De Feyter, *Chem. Commun.*, 2021, **57**, 962–977.
4 M. Liu, L. Zhang and T. Wang, *Chem. Rev*. 2015, **115**, 7304–7397.
5 S. Huang, H. Yu and Q. Li, *Adv. Sci.*, 2021, **8**, 2002132.
6 J. Dong, Y. Liu and Y. Cui, *Acc. Chem. Res*. 2021, **54**, 194–206.
7 L.-J. Chen, H.-B. Yang and M. Shionoya, *Chem. Soc. Rev.*, 2017, **46**, 2555–2576.
8 T. Tateishi, T. Kojima and S. Hiraoka, *Commun. Chem*. 2018, **1**, 20.
9 P. Xing and Y. Zhao, *Acc. Chem. Res*. 2018, **51**, 2324–2334.
10 M. Hifsudheen, R. K. Mishra, B. Vedhanarayanan, V. K. Praveen and A. Ajayaghosh, *Angew. Chem., Int. Ed.*, 2017, **56**, 12634–12638.
11 C. Kulkami, J. A. Berrocal, M. Lutz, A. R. A. Palmans and E. W. Meijer, *J. Am. Chem. Soc.*, 2019, **141**, 6302–6309.
12 D. K. Smith, *Chem. Soc. Rev*. 2009, **38**, 684–694.
13 D. P. Goronzy, M. Ebrahimi, F. Rosei, Arramel, Y. Fang, S. De Feyter, S. L. Tait, C. Wang, P. H. Beton, A. T. S. Wee, P. S. Weiss and D. F. Perepichka, *ACS Nano*, 2018, **12**, 7445–7481.
14 F. Zaera, *Chem. Soc. Rev*. 2017, **46**, 7374–7398.
15 K. S. Mali, N. Pearce, S. De Feyter and N. R. Champness, *Chem. Soc. Rev.*, 2017, **46**, 2520–2542.
16 J. W. Huan, X. M. Zhang and Q. D. Zeng, *Phys. Chem. Chem. Phys.*, 2019, **21**, 11537–11553.
17 Y. Xu, J.-J. Duan, Z.-Y. Yi, K.-X. Zhang, T. Chen and D. Wang, *Surf. Sci. Rep*., 2021, **76**, 100531.
18 R. Raval, *Chem. Soc. Rev*. 2009, **38**, 707–721.
19 S. Dutta and A. J. Gellman, *Chem. Soc. Rev*. 2017, **46**, 7787–7839.
20 K.-H. Ernst, *Phys. Status Solidi B* 2012, **249**, 2057–2088.
21 D. B. Amabilino, *Chirality at the Nanoscale. Nanoparticles, Surfaces, Materials and more*. Wiley-VCH Verlag GmbH & Co. kGaA, Weinheim, 2009, 1–28.
22 K. Tahara, H. Yamaga, E. Ghijsens, K. Inukai, J. Adisoejoso, M. O. Blunt, S. De Feyter and Y. Tobe, *Nat. Chem.*, 2011, **3**, 714–719.
23 K. Tahara, A. Noguchi, R. Nakayama, E. Ghijsens, S. De Feyter and Y. Tobe, *Angew. Chem., Int. Ed.*, 2019, **58**, 7733–7738.
24 T. Chen, W. H. Yang, D. Wang and L. J. Wan, *Nat. Commun.*, 2013, **4**, 1389–1396.
25 I. Destoop, A. Minoia, O. Ivasenko, A. Noguchi, K. Tahara, Y. Tobe, R. Lazzaroni and S. De Feyter, *Faraday Discuss.*, 2017, **204**, 215–231.
26 S. Xue, P. Xing, J. Zhang, Y. Zeng and Y. Zhao, *Chem. – Eur. J.*, 2019, **25**, 7426–7437.
27 Y. L. Wang, K. Sun, Y. B. Tu, M. L. Tao, Z. B. Xie, H. K. Yuan, Z. H. Xiong and J. Z. Wang, *Phys. Chem. Chem. Phys.*, 2018, **20**, 7125–7131.
28 T. Chen, S.-Y. Li, D. Wang and L.-J. Wan, *Sci. Adv.*, 2017, **3**, 1701208–1701215.
29 Y. Fang, E. Ghijsens, O. Ivasenko, H. Cao, A. Noguchi, K. S. Mali, K. Tahara, Y. Tobe and S. De Feyter, *Nat. Chem.*, 2016, **8**, 711–717.
30 H. Cao and S. De Feyter, *Nat. Commun*. 2018, **9**, 3416.
31 J. Labella, G. Lavarda, L. Hernández-López, F. Aguilar-Galindo, S. Díaz-Tendero, J. Lobo-Checa and T. Torres, *J. Am. Chem. Soc.*, 2022, **144**, 16579–16587.
32 H. Zhang, Z. Gong, K. Sun, R. Duan, P. Ji, L. Li, C. Li, K. Müllen and L. Chi, *J. Am. Chem. Soc.*, 2016, **138**, 11743–11748.
33 C. Lu, Y.-P. Mo, Y. Hong, T. Chen, Z.-Y. Yang, L.-J. Wan and D. Wang, *J. Am. Chem. Soc.*, 2020, **142**, 14350–14356.
34 K. Tahara, Y. Kubo, S. Hashimoto, T. Ishikawa, H. Kaneko, A. Brown, B. E. Hirsch, S. D. Feyter and Y. Tobe, *J. Am. Chem. Soc.*, 2020, **142**, 7699–7708.
35 Y. Chen, K. Deng, S. Lei, R. Yang, T. Li, Y. Gu, Y. Yang, X. Qiu and C. Wang, *Nat. Commun.*, 2018, **9**, 2711.
36 C. Li, R. Li, Z. Xu, J. Li, X. Zhang, N. Li, Y. Zhang, Z. Shen, H. Tang and Y. Wang, *J. Am. Chem. Soc.*, 2021, **143**, 14417–14421.
37 D. Cui, J. M. MacLeod and F. Rosei, *Chem. Commun.*, 2018, **54**, 10527–10539.
38 S. De Feyter and F. C. De Schryver, *J. Phys. Chem. B*, 2005, **109**, 4290–4302.
39 J. Liu, T. Chen, X. Deng, D. Wang, J. Pei and L.-J. Wan, *J. Am. Chem. Soc.*, 2011, **133**, 21010–21015.
40 S. Lei, M. Surin, K. Tahara, J. Adisoejoso, R. Lazzaroni, Y. Tobe and S. De Feyter, *Nano Lett.*, 2008, **8**, 2541–2546.
41 Y. Xue and M. B. Zimmt, *J. Am. Chem. Soc.*, 2012, **134**, 4513–4516.
42 M. Lal Saha and M. Schmittel, *Org. Biomol. Chem*. 2012, **10**, 4651–4684.

43 M. M. Safont-Sempere, G. Fernández and F. Würthner, *Chem. Rev.*, 2011, **111**, 5784–5814.
44 Q. Liu, B. Jin, Q. Li, H. Yang, Y. Luo and X. Li, *Soft Matter*, 2022, **18**, 2484–2499.
45 Z. He, W. Jiang and C. A. Schalley, *Chem. Soc. Rev.*, 2015, **44**, 779–789.
46 W. Xiao, X. Feng, P. Ruffieux, O. Gröning, K. Müllen and R. Fasel, *J. Am. Chem. Soc.*, 2008, **130**, 8910–8912.
47 S. Clair, M. Abel and L. Porte, *Angew. Chem., Int. Ed*. 2010, **49**, 8237–8239.
48 Y. Ye, W. Sun, Y. Wang, X. Shao, X. Xu, F. Cheng, J. Li and K. Wu, *J. Phys. Chem. C*, 2007, **111**, 10138–10141.
49 J. Zhang, B. Li, X. F. Cui, B. Wang, J. L. Yang and J. G. Hou, *J. Am. Chem. Soc.*, 2009, **131**, 5885–5890.
50 T. Jasper-Tonnies, M. Gruber, S. Ulrich, R. Herges and R. Berndt, *Angew. Chem., Int. Ed.*, 2020, **59**, 7008–7017.
51 J. Lu, H. Jiang, Y. Yan, Z. Zhu, F. Zheng and Q. Sun, *ACS Nano*, 2022, **16**, 13160–13167.
52 S. S. Jester, E. Sigmund, L. M. Röck and S. Höger, *Angew. Chem., Int. Ed.*, 2012, **51**, 8555–8559.
53 M. Maeda, R. Nakayama, S. De Feyter, Y. Tobe and K. Tahara, *Chem. Sci.*, 2020, **11**, 9254–9261.
54 J. Zhang, A. Gesquière, M. Sieffert, M. Klapper, K. Müllen, F. C. De Schryver and S. De Feyter, *Nano Lett.*, 2005, **5**, 1395–1398.
55 C. Karageorgaki and K.-H. Ernst, *Chem. Commun.* 2014, **50**, 1814–1816.
56 I. De Cat, Z. Guo, S. J. George, E. W. Meijer, A. P. H. J. Schenning and S. De Feyter, *J. Am. Chem. Soc.*, 2012, **134**, 3171–3177.
57 W. Song, N. Martsinovich, W. M. Heckl and M. Lackinger, *J. Am. Chem. Soc.*, 2013, **135**, 14854–14862.